

# Orbital interaction mechanisms of conductance enhancement and rectification by dithiocarboxylate anchoring group

Zhenyu Li and D. S. Kosov

*Department of Chemistry and Biochemistry,  
University of Maryland, College Park, MD 20742*

## Abstract

We study computationally the electron transport properties of dithiocarboxylate terminated molecular junctions. Transport properties are computed self-consistently within density functional theory and non-equilibrium Green's functions formalism. A microscopic origin of the experimentally observed current amplification by dithiocarboxylate anchoring groups is established. We find that for the 4,4'-biphenyl bis(dithiocarboxylate) junction the interaction of LUMO of the dithiocarboxylate anchoring group with LUMO and HOMO of the biphenyl part results into bonding and antibonding resonances in the transmission spectrum in the vicinity of the electrode Fermi energy. A new microscopic mechanism of rectification is predicted based on the electronic structure of asymmetrical anchoring groups. We show that peaks in the transmission spectra of 4'-thiolato-biphenyl-4-dithiocarboxylate junction respond differently to the applied voltage. Depending upon the origin of a transmission resonance in the orbital interaction picture, its energy can be shifted along with the chemical potential of the electrode to which the molecule is stronger or weaker coupled.

## I. INTRODUCTION

One of the main goals in nanotechnology is the construction, measurement and modeling of electronic circuits in which molecular systems act as conducting elements.<sup>1,2</sup> When a molecule is attached to two macroscopic metal electrodes with different chemical potentials, the electric current flows through it. The coupling to electrodes mixes the discrete molecular levels with the continuum of the metal electronic states such that the molecular orbitals protrude deep inside the electrode. The coupling also renormalizes the energies of the molecular orbitals. Therefore, it is no longer correct to talk about the transport properties of the molecule, but rather, only of the electrode-molecule-electrode heterojunction. If the strength of the molecule-electrode coupling is large, substantial perturbation of the molecular electronic structure can occur. In fact, it is expected that upon initial chemisorption, substantial charge transfer takes place between the metal electrode and the molecule even in the absence of an applied voltage bias. These effects are pivotal for molecular wire transport properties and they can be controlled by changing the interface geometry or by altering the anchoring groups, which provide the linkage between the molecule and the electrode.<sup>3,4,5,6,7,8,9,10</sup> Therefore the study of the anchoring group chemistry in molecular electronics may help us not only to pin down the origin of significant discrepancy between experimental and theoretical molecular conductivities but may also reveal new fascinating fundamental aspects of molecule-surface interactions. With only a few exceptions,<sup>11,12,13</sup> the most widely used molecular wire junctions have been formed so far by organic molecules assembled between gold electrodes via thiol anchoring groups. However, thiol linkage is considered to be only structural and lacks any subsequent useful "chemistry",<sup>12</sup> since the energy and the electron occupation of sulfur 3p orbital is difficult to modify. Tulevski *et al.*<sup>12</sup> thus suggested to use ruthenium electrode instead of gold. But being excellent conductor and metal with mature manipulation techniques, gold remains the most attractive electrode material.

The quest for reliable molecular electronic devices has become the search for better molecule-gold linkers,<sup>14</sup> which provide the opportunity not only to grow the single molecular contacts but also to control molecular transport properties. Recently, Tivanski *et al.*<sup>15</sup> suggested and realized experimentally the remarkable molecular wire, which is attached to the gold electrodes via dithiocarboxylate conjugated linker (-CS<sub>2</sub>). The conductance of 4,4'-

biphenyl dithiolate (BDT) and 4,4'-biphenyl bis(dithiocarboxylate) (BDCT) molecular wires were measured by conducting-probe atomic force microscopy.<sup>15</sup> The central conducting parts of both BDT and BDCT are exactly the same (biphenyl) whereas the anchoring groups are different. BDT has the standard thiol groups and BDCT is terminated by dithiocarboxylate groups. It was experimentally observed that the conductance of BDCT is 1.4 times as large as that of BDT.<sup>15</sup> But the physical origin of this conductance enhancement was not clear. The most intuitive picture suggests that the conjugated dithiocarboxylate anchoring group provides the stronger coupling between the electrode and the molecule.<sup>15</sup> We have recently demonstrated that this simple mechanism plays a central role in conductance enhancement induced by dithiocarbamate linker (N-CS<sub>2</sub>),<sup>10</sup> where the stronger molecule-electrode coupling leads to the larger mixing between the discrete molecular levels and the continuum of the metal electronic states, and thus to the larger broadening of resonances in the electron transmission spectrum. As it turned out the mechanism of the conductance enhancement is entirely different for dithiocarbamate and dithiocarboxylate linkers, although they are structurally very similar. One of the aims of this paper is to elucidate the microscopic origin of the conductance enhancement via dithiocarboxylate linkers. We show that the reason for the conductance enhancement is not simply the difference in the molecule-electrode coupling strengths but the disparity in the electronic structure of thiol and dithiocarboxylate anchoring groups.

One of the interesting possibilities, which we also would like to explore in our paper, is the use of dithiocarboxylate linkers to create a molecular rectifier. A molecular rectifier is a junction where electrons flow along one preferential direction.<sup>16,17</sup> As a prototype molecular junction we consider biphenyl with thiol linker on one side and with dithiocarboxylate anchoring group on the other – 4'-thiolato-biphenyl-4-dithiocarboxylate – (TBCT). Rectification for molecules with asymmetric anchoring groups has been studied theoretically,<sup>10,18</sup> however, in all junctions considered so far the role of anchoring groups was limited to providing left-right asymmetry in the coupling strength between the molecule and the electrodes. It leads to the standard coupling-strength picture of molecular rectification, which predicts that as the voltage bias increases the peaks in the transmission are shifted along with the chemical potential of the electrode to which the molecule is stronger coupled.<sup>10,18</sup> Suppose that, for example, there are two resonances in the transmission spectrum in the vicinity of the electrode Fermi energy with the energies above and below it, so that both resonances

contribute to the electron transport at moderate voltages. Within the standard rectification picture the two peaks are shifted in the same direction.<sup>10,18</sup> Therefore, when the energy of one resonance enters the integration range between the chemical potentials of the left and the right electrodes (i.e. it starts to contribute to the electron current) the second resonance could be already shifted away from the integration range. Thus, as soon as the contribution from one peak to the current increases, the role of the second pick decreases. This counterbalancing reduces the rectification effects within the standard coupling-strength mechanism. In this paper we show that the TBCT molecular junction exhibits an entirely new mechanism of rectification, which overcomes the limitations of the standard coupling strength picture described above.

The remainder of the paper is organized as follows. In section II, we describe the computational details. The main results are discussed in section III. We first illustrate how the electronic structure of thiol and dithiocarboxylate anchoring groups control and determine transport properties of molecular wire junctions. A new rectification mechanism is suggested for molecule attached to electrodes by thiol and dithiocarboxylate groups. Section IV concludes the paper

## II. COMPUTATIONAL METHODS

Two computer programs were used in our calculations. First, optimized geometries of the molecular junctions were obtained by SIESTA computer program.<sup>19</sup> Then electron transport properties were computed by using TranSIESTA-C package.<sup>20</sup> TranSIESTA-C uses the combination of non-equilibrium Green's function (NEGF) formalism and density functional theory (DFT). In NEGF theory, the molecular wire junction is divided into three regions: left electrode (L), contact region (C), and right electrode (R). The semi-infinite electrodes are calculated separately to obtain the bulk self-energy. The contact region contains parts of the electrodes to include the screening effects in the calculations. The electrodes are modeled by semi-infinite Au surfaces. The main loop for TranSIESTA-C self-consistent NEGF/DFT calculations is described below (for technical details we refer to paper<sup>20</sup>). The matrix product of the Green's function and the imaginary part of the left/right electrode self-energy yields the spectral densities. The spectral densities of the left and right electrodes are combined together to compute the nonequilibrium, voltage-dependent density

matrix and then the density matrix is converted into nonequilibrium electron density. The nonequilibrium electron density enables us to compute matrix elements of Green's function. The Hartree potential is determined through the solution of the Poisson equation with appropriate voltage-dependent boundary conditions. This loop of calculations is repeated until self-consistency is achieved. After the self-consistent convergence is achieved, the voltage transmission spectrum is calculated by the standard equation

$$T(E, V) = \text{Tr}[\mathbf{\Gamma}_L(E, V)\mathbf{G}(E, V)\mathbf{\Gamma}_R(E, V)\mathbf{G}^\dagger(E, V)], \quad (1)$$

where  $\mathbf{G}$  is the Green's function of the contact region,  $\mathbf{\Gamma}_{L/R}$  is the coupling matrix, and  $V$  is the applied voltage bias. The electric current as a function of the applied voltage is obtained by the integration of the transmission spectrum.

$$I(V) = (-e) \int T(E, V)(f(E - \mu_L) - f(E - \mu_R))dE, \quad (2)$$

where  $f$  is the Fermi-Dirac occupation number,  $\mu_L = -eV/2$  ( $\mu_R = eV/2$ ) is the chemical potential for the left (right) electrode and  $e$  is the elementary charge.

We use double- $\zeta$  with polarization (DZP) basis for all atoms except Au, for which single- $\zeta$  with polarization (SZP) is used. We use Troullier-Martins nonlocal pseudopotentials in all our calculations.<sup>21</sup> The exchange-correlation potential is described by Perdew-Zunger local density approximation (LDA).<sup>22</sup> Single  $k$ -point sampling on the plane perpendicular to the direction of the current is used in our calculations. Our tests show that the generalized gradient approximation<sup>23</sup> yields negligible corrections to the LDA transmission spectra and the use of  $4 \times 4$   $k$ -point sampling does not affect main features of the transmissions.

### III. RESULTS AND DISCUSSION

#### A. Structural model of molecular junctions

We consider three representative molecular wire junction systems: BDT, BDCT, and TBCT. BDT and BDCT are terminated by thiol and dithiocarboxylate respectively on both ends. In TBCT, dithiocarboxylate group is used on the left side while thiol group is used on the right side. Figure 1 shows the optimized junction geometries. The semi-infinite left and right electrodes are modeled by two Au(111)-(3 $\times$ 3) surfaces, for which only one unit cell (contains three Au layers) is plotted. In the contact region, two Au layers at both left

and right side are included. The outmost left and right layers in the contact regions are constrained to their theoretical bulk geometry to match the structure of Au(111)-(3×3) surfaces which are used to model the electrodes. We assume the biphenyl interior part of all three junctions have coplanar geometry. This narrows down the problem of difference between BDT, BDCT and TBCT transport properties to the role of the dithiocarboxylate linkers. The rest of the contact region is fully optimized. We also optimized the length of the junctions by computing the total energies of the systems as functions of the distance between the left and the right electrodes. Every single energy point is calculated by performing geometry optimization with constrained electrode-electrode separation. The optimal separation between the electrodes is obtained as the distance at which the total energy is minimal. We also perform test calculations for non-coplanar BDT and BDCT. The twisting of phenyl rings by 37°, which corresponds to the equilibrium geometry for biphenyl junction,<sup>6</sup> has negligible influence on the transmission spectra. The twisting merely reduces the overall transmission probability without any further alternation of the transmission spectra.

## B. Orbital interaction mechanism of conductance enhancement

With the optimized geometries, we calculate transmission spectra and current-voltage (I-V) characteristics for BDT and BDCT, as shown in Figure 2. The computed current is four orders of magnitude larger than the experimental one.<sup>15</sup> Our I-V curves qualitatively reproduce the experimental conductance enhancement although theoretically predicted increase in conductivity ( $\sim 2.1$ ) is larger than the experimentally observed amplification factor ( $\sim 1.4$ ).<sup>15</sup> The conductance enhancement is clearly shown in the transmission spectra. For BDT, there are two broad peaks: one is below the electrode Fermi energy ( $\sim -0.8$  eV) and the other is above it ( $\sim 2.1$  eV). These two peaks can still be found in the transmission spectrum of BDCT, but the first peak is shifted toward the lower energy ( $\sim -1.5$  eV) and the second peak is moved to the higher energy ( $\sim 2.9$  eV). Besides these two peaks, the additional broad peak appears for BDCT just above the Fermi energy. It gives almost perfect transmission probability in the broad energy range from 0.1 to 1.1 eV. This broad peak results in large transmission probability at the Fermi energy and is responsible for the conductance enhancement for BDCT junction observed on experiment.<sup>15</sup>

The microscopic origin of this broad peak and thus the cause of the conductance enhance-

ment can be understood from the partitioning of the transport channels into contribution from the interior part (biphenyl) and the linkers (thiol or dithiocarboxylate). If we project the self-consistent hamiltonian onto the Hilbert space spanned by the basis functions of the molecule (includes biphenyl and anchoring groups), we obtain the molecular projected self-consistent hamiltonian (MPSH). The eigenstates of MPSH can be considered as molecular orbitals renormalized by the molecule-electrode interaction. Figure 3 shows the MPSH orbitals near the Fermi level of the electrodes and Table I shows the corresponding eigenvalues. Comparing the energies of the resonances in the transmission spectra with the eigenvalues of MPSH, we find that the two main transmission peaks of BDT are mainly contributed by MPSH orbitals 34 and 35, while the peaks of BDCT take their origin from MPSH orbitals 44, 45, 46, and 48. The common feature of these orbitals is the significant de-localization and spread of the electron density along the interior region of the wire as well as the anchoring groups. The additional peak in the transmission spectrum of BDCT is not a single broad resonance. As is elucidated by the MPSH analysis, the merging of two resonances from MPSH orbitals 45 and 46 produces this broad peak. Peaks in BDTC transmission do not show significant additional broadening with respect to BDT resonances.

The MPSH orbitals can be further disentangled if we consider them as generated by the interaction between orbitals localized on the anchoring groups and orbitals of the interior part (biphenyl molecule). Dissecting all relevant MPSH orbitals for the three junctions shows that all of them can be obtained from linear combinations of the two anchoring group orbitals (sulphur  $3p$  orbital of thiol linkage and LUMO of dithiocarboxylate) and the HOMO/LUMO of biphenyl molecule. This orbital interaction picture is presented in Figure 4. The biphenyl HOMO and LUMO (orbital 28 and 29 in Table I), are labeled as  $\epsilon_1^M$  and  $\epsilon_2^M$  in Figure 4. Sulfur  $3p$  atomic orbital of thiol linkage ( $\epsilon^S$ ) lays very deep (-2.88 eV from calculation of atomic energy levels of sulphur) below the Fermi energy of the gold surface.<sup>12</sup> When thiol group is attached to biphenyl, the resulted MPSH orbitals are all far from the Fermi level, and only the anti-bonding orbitals ( $\epsilon_3$  and  $\epsilon_4$ ) contribute to low voltage electron transport. From Fig. 3a, we can easily identify  $\epsilon_3$  and  $\epsilon_4$  as BDT MPSH orbitals 34 and 35 respectively.

The orbital interaction picture leads to very different mechanism of electron transport through BDCT molecular wire. Here, orbital interaction between the LUMO of the dithiocarboxylate group ( $\epsilon^{CT}$ ) and the biphenyl HOMO/LUMO contributes to the four resonance

structures in the transmission spectrum. The value of  $\epsilon^{CT}$  (0.35 eV from calculation of  $\text{H}_2\text{S}_2\text{-CH}$  molecular orbitals) is much higher than  $\epsilon^S$  in the thiol, and, therefore, both bonding and anti-bonding MPSH orbitals of BDCT are positioned in the vicinity of the Fermi energy and contribute to low bias electron transport. The right side of Figure 4 shows the orbital interaction picture for BDCT, where levels  $\epsilon'_1$  to  $\epsilon'_4$  correspond to MPSH orbital 44, 45, 46, and 48 respectively. Level  $\epsilon'_2$ , which is almost in resonance with the electrode Fermi energy, gives the main contribution to low voltage electron transport. Therefore, it is the intrinsic electronic structure difference between the anchoring groups that is the real origin for the observed conductance enhancement by the dithiocarboxylate anchoring group.

### C. Rectification

In this section, we demonstrate that the biphenyl molecular wire with thiol linker on one side and dithiocarboxylate anchoring group on the other (TBCT) exhibits a new mechanism of rectification. The mechanism enables us to overcome the limitation of the standard coupling-strength picture,<sup>10,18</sup> in which rectification from one resonance could be reduced by the opposite contribution from another resonance.

The voltage dependence of the transmission spectrum of TBCT junction shows very complicated patterns (Figure 5 and Table II). There are three main transmission peaks. The left peak (A) shifts toward the higher energy as the voltage changes from negative to positive bias, the middle peak (B) shows the opposite behavior, and the right peak (C) does not shift at all. It means that peak A follows the changes in the chemical potential of the right electrode ( $\mu_R = eV/2$ ), while peak B follows the chemical potential of the left electrode ( $\mu_L = -eV/2$ ). The current-voltage characteristics is shown in the inset of Figure 5. It is obtained by integrating the transmission from  $\mu_L$  to  $\mu_R$ . For negative bias voltage, both peaks A and B are not within the integration range, therefore the current is small. Under positive voltage, when the value of the voltage increases, both A and B enter the integration region and produce large current increase. We thus obtain rectification coefficient  $R = I(V)/I(-V) \sim 2.8$  at 1.0 eV bias voltage.

The response of the transmission spectrum on the applied voltage bias can be readily understood if we look at the MPSH orbitals as plotted in Figure 3c. Peaks A, B, and C correspond to MPSH orbitals 39, 40, and 41 respectively. Orbital 39 has stronger molecule-

electrode coupling via the thiol group so that the energy of this orbital follows the chemical potential of the right electrode. This orbital is mainly antibonding mixture of the HOMO of biphenyl ( $\epsilon_1^M$  in Fig. 4) and  $3p$  orbital of the sulphur ( $\epsilon^S$ ). Therefore orbital 39 ( $\epsilon_3$  plus minor contribution from  $\epsilon_1'$ ) has stronger coupling at the thiol side. Similarly, orbital 40 is mainly related to  $\epsilon_2'$ , which has stronger coupling via the dithiocarboxylate group and follows the chemical potential of the left electrode. Orbital 41 is anti-bonding at both sides, and can be considered as combination of  $\epsilon_4$  and  $\epsilon_4'$ . It interacts equally well with both electrodes. Therefore the influence of the left electrode is balanced by the influence of the right electrode and this orbital is not significantly affected by the applied voltage. To summarize, likewise in the case of the conductance enhancement, the electronic structure of the anchoring groups and orbital interaction picture provide the explanation why these three transmission peaks behave differently under the voltage bias.

Schematic diagram which shows the qualitative behavior of the two peaks is presented on Figure 6. In the standard coupling-strength picture, all transmission peaks follow the chemical potential of the stronger coupled electrode (left electrode in the figure).<sup>10,18</sup> If there are two transmission peaks equally spaced below and above the mean Fermi level of the electrode (A and B on Figure 6) their contributions to the rectification counteract each other. At negative bias, peak A enters the integration range, which increases the current comparing to that at the positive bias. The current prefers to flow from the right to the left due to peak A. On the other hand, peak B increases the current at positive bias voltage, and, therefore the current prefers to flow the left to right because of peak B. This situation can be avoided in the orbital interaction picture, where peaks A and B respond oppositely on the applied voltage. As shown in the right part of Figure 6, which is exactly the situation we find in the TBCT junction, where both peaks A and B rectify the current in the same direction.

#### IV. CONCLUSIONS

We have performed DFT-NEGF calculations to elucidate the microscopic origin of the conductance enhancement via dithiocarboxylate linkers. We showed that the reason for the conductance enhancement is not simply the difference in the molecule-electrode coupling strengths but the disparity in the electronic structure of thiol and dithiocarboxylate anchor-

ing groups. We suggested the use of dithiocarboxylate linker to create a molecular rectifier. As a prototype molecular rectifier we considered a biphenyl with a thiol linker on one side and with a dithiocarboxylate anchoring group on the other (TBCT molecule). We predicted that the TBCT molecular junction exhibits an entirely new mechanism of rectification which had never been predicted theoretically or observed experimentally before. Our calculations demonstrate how electronic structure of anchoring groups accompanied by molecular orbital interaction picture can be used as a guiding principle to predict transport properties of molecular junctions.

### **Acknowledgments**

The authors are grateful to M. Gelin, L. Sita, A. Vedernikov, and J. Yang for helpful discussion. This work was partially supported by the American Chemical Society Petroleum Research Fund (44481-G6) and by summer award of General Research Board of the University of Maryland.

### **Supporting Information Available**

Total energies of the molecular junctions as functions of electrode-electrode separation, transmission spectra for different molecular geometries, transmission spectra computed with GGA exchange-correlation functional, and transmission spectra computed with  $4 \times 4$   $k$  sampling. This material is available free of charge via the Internet at <http://pubs.acs.org>.

- 
- <sup>1</sup> Nitzan, A.; Ratner, M. A. *Science* **2003**, 300, 1384.
- <sup>2</sup> Joachim, C.; Ratner, M. A. *Proc. Natl. Acad. Sci. U.S.A.* **2005**, 102, 8801.
- <sup>3</sup> Venkataraman, L.; Klare, J. E.; Tam, I. W.; Nuckolls, C.; Hybertsen, M. S.; Steigerwald, M. L. *Nano Lett.* **2006**, 6, 458.
- <sup>4</sup> Li, X.; He, J.; Hihath, J.; Xu, B.; Lindsay, S. M.; Tao, N. *J. Am. Chem. Soc.* **2006**, 128, 2135.
- <sup>5</sup> Kim, B.; Beebe, J. M.; Jun, Y.; Zhu, X.-Y.; Frisbie, C. D. *J. Am. Chem. Soc.* **2006**, 128, 4970.
- <sup>6</sup> Xue, Y.; Ratner, M. A. *Phys. Rev. B* **2003**, 68, 115406.
- <sup>7</sup> Ke, S.-H.; Baranger, H. U.; Yang, W. *J. Am. Chem. Soc.* **2004**, 126, 15897.
- <sup>8</sup> Basch, H.; Cohen, R.; Ratner, M. A. *Nano Lett.* **2005**, 5, 1668.
- <sup>9</sup> Ke, S.-H.; Baranger, H. U.; Yang, W. *J. Chem. Phys.* **2005**, 123, 114701.
- <sup>10</sup> Li, Z.; Kosov, D. S. *J. Phys. Chem. B* **2006**, 110, 9893.
- <sup>11</sup> Siaj, M.; McBreen, P. H. *Science* **2005**, 309, 588.
- <sup>12</sup> Tulevski, G. S.; Myers, M. B.; Hybertsen, M. S.; Steigerwald, M. L., Nuckolls, C. *Science* **2005**, 309, 591.
- <sup>13</sup> Guo, X. et al., *Science* **2006**, 311, 356.
- <sup>14</sup> Akkerman, H. B.; Blom, P. W. M.; de Leeuw, D. M.; de Boer B. *Nature* **2006**, 441, 69.
- <sup>15</sup> Tivanski, A. V.; He, Y.; Borguet, E.; Liu, H.; Walker, G. C.; Waldeck, D. H. *J. Phys. Chem. B* **2005**, 109, 5398.
- <sup>16</sup> Aviram, A.; Ratner, M. A. *Chem. Phys. Lett.* **1974**, 29, 277-283.
- <sup>17</sup> Metzger, R. M. *Chem. Rev.* **2003**, 103, 3803.
- <sup>18</sup> Taylor, J.; Brandbyge, M.; Stokbro, K. *Phys. Rev. Lett.* **2002**, 89, 138301.
- <sup>19</sup> Soler, J. M.; Artacho, E., Gale, J.; Garcia, A., Junquera, J.; Ordejon, P.; Sanchez-Portal, D. *J. Phys.: Condens. Matter* **2002**, 14, 2745-2779.
- <sup>20</sup> Brandbyge, M.; Mozos, J.-L.; Ordejon, P.; Taylor, J.; Stokbro, K. *Phys. Rev. B* **2002**, 65, 165401.
- <sup>21</sup> Troullier, N; Martins, J. L. *Phys. Rev. B* **1991**, 43, 1993.
- <sup>22</sup> Perdew, J. P.; Zunger, A. *Phys. Rev. B* **1981**, 23, 5048.
- <sup>23</sup> Perdew, J. P.; Burke, K.; Ernzerhof, M. *Phys. Rev. Lett.* **1996**, 77, 3865.

TABLE I: Energies of molecular orbitals of biphenyl and MPSH orbitals of BDT, BDCT, and TBDT. All energies are relative to the Fermi energy of the gold electrode.

Biphenyl		BDT		BDCT		TBDT	
$n$	$\epsilon_n(\text{eV})$	$n$	$\epsilon_n(\text{eV})$	$n$	$\epsilon_n(\text{eV})$	$n$	$\epsilon_n(\text{eV})$
25	-3.926	31	-2.580	43	-2.222	37	-2.343
26	-3.201	32	-2.433	44	-1.821	38	-2.230
27	-3.052	33	-2.341	45	0.003	39	-1.489
28	-2.358	34	-1.271	46	0.849	40	0.433
29	1.229	35	1.838	47	2.772	41	2.305
30	1.840	36	2.506	48	2.808	42	2.559
31	2.350	37	3.020	49	3.257	43	3.087

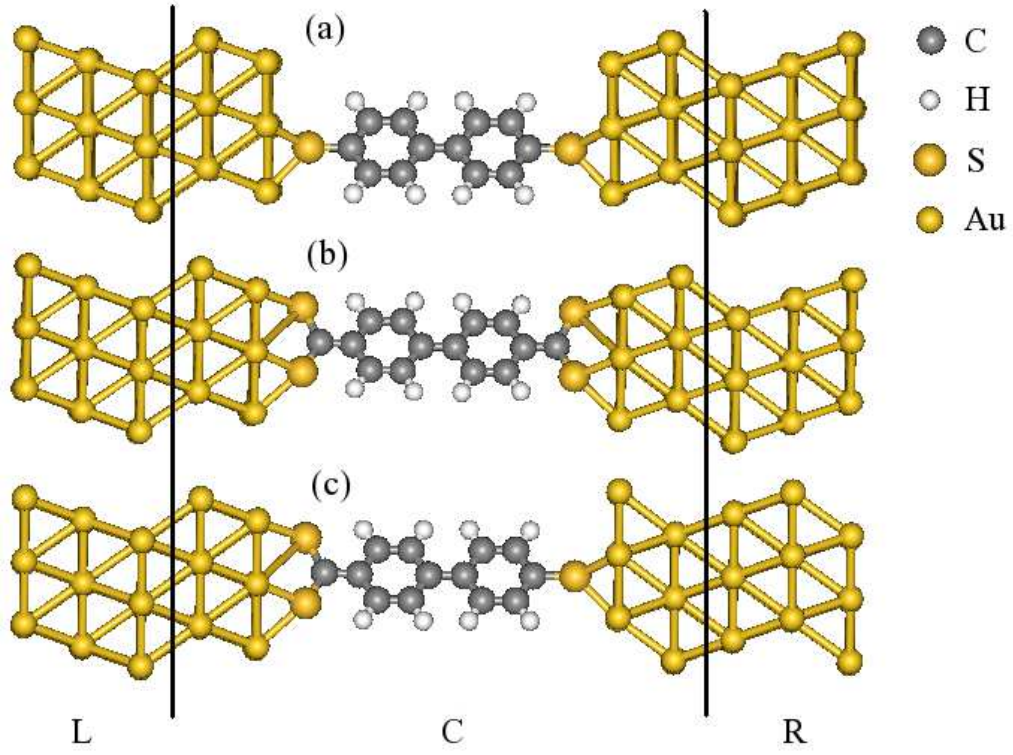


FIG. 1: Relaxed geometry of molecular wire junctions with different anchoring groups. (a) BDT, (b) BDCT, (c) TBCT. Only one unit cell for the semi-infinite electrode is plotted.

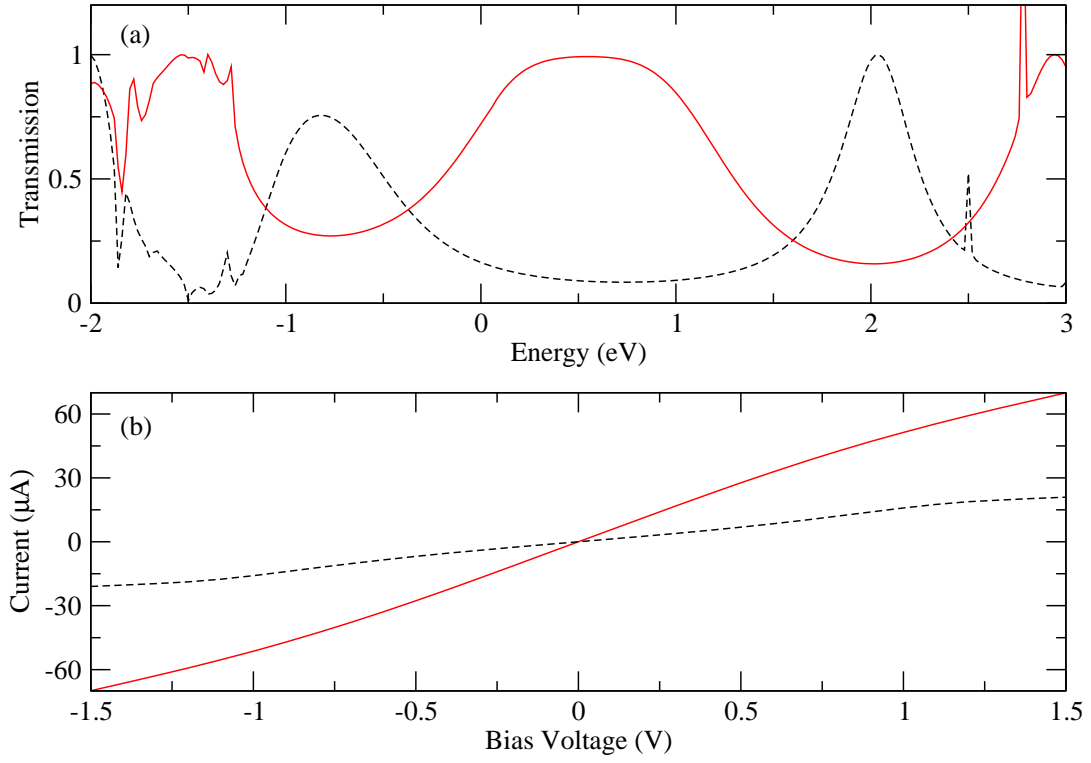


FIG. 2: (a) Zero voltage bias transmission spectra and (b) current-voltage characters of BDT (dashed) and BDCT (solid) molecular junctions. Fermi energy of the electrode is set to zero in the transmission spectra.

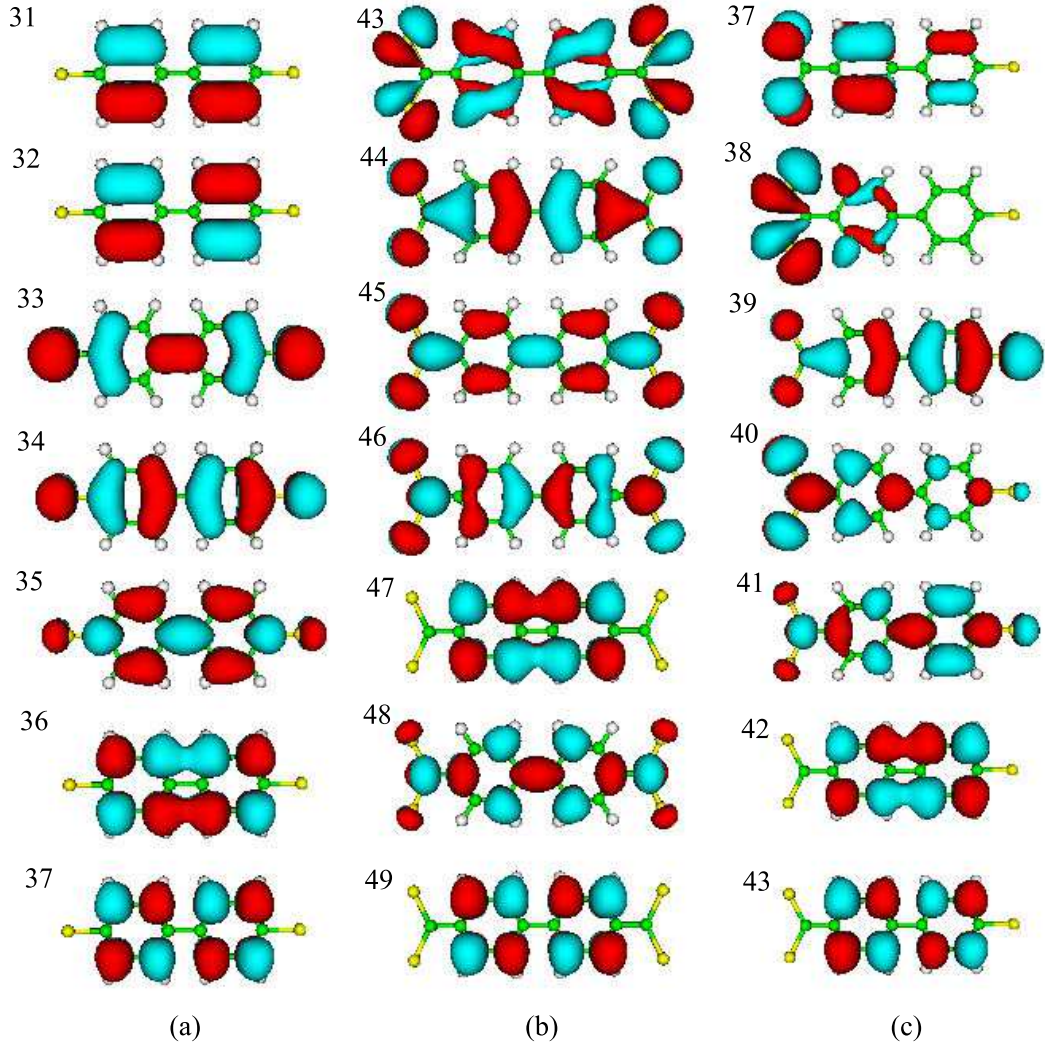


FIG. 3: MPSH orbitals near gold electrode Fermi level for (a) BDT, (b) BDCT, and (c) TBCT.

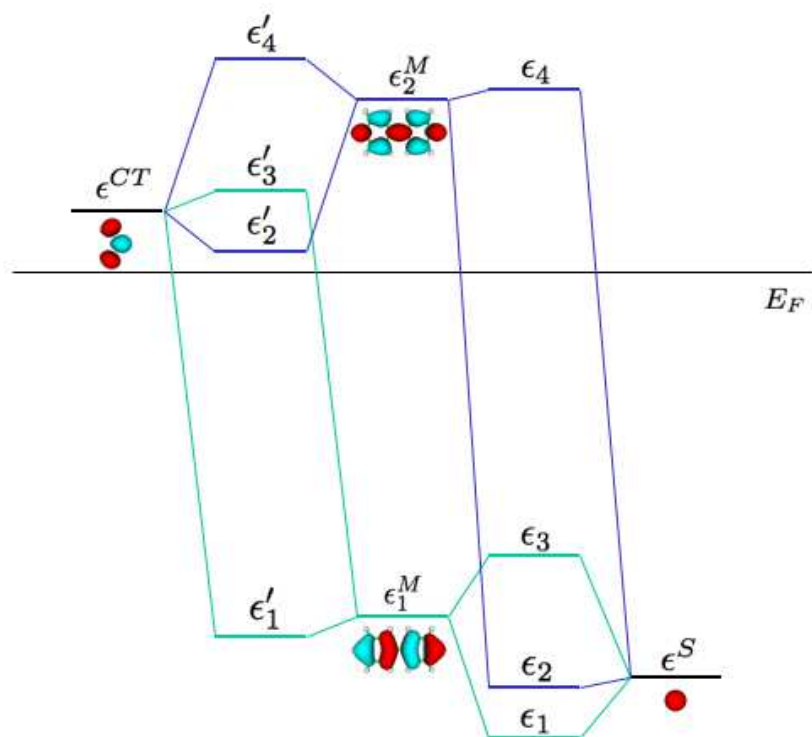


FIG. 4: Schematic orbital interaction picture. Interaction between biphenyl HOMO/LUMO and anchoring group orbitals (sulphur  $p$  and dithiocarboxylate LUMO) leads to MPSH orbitals.

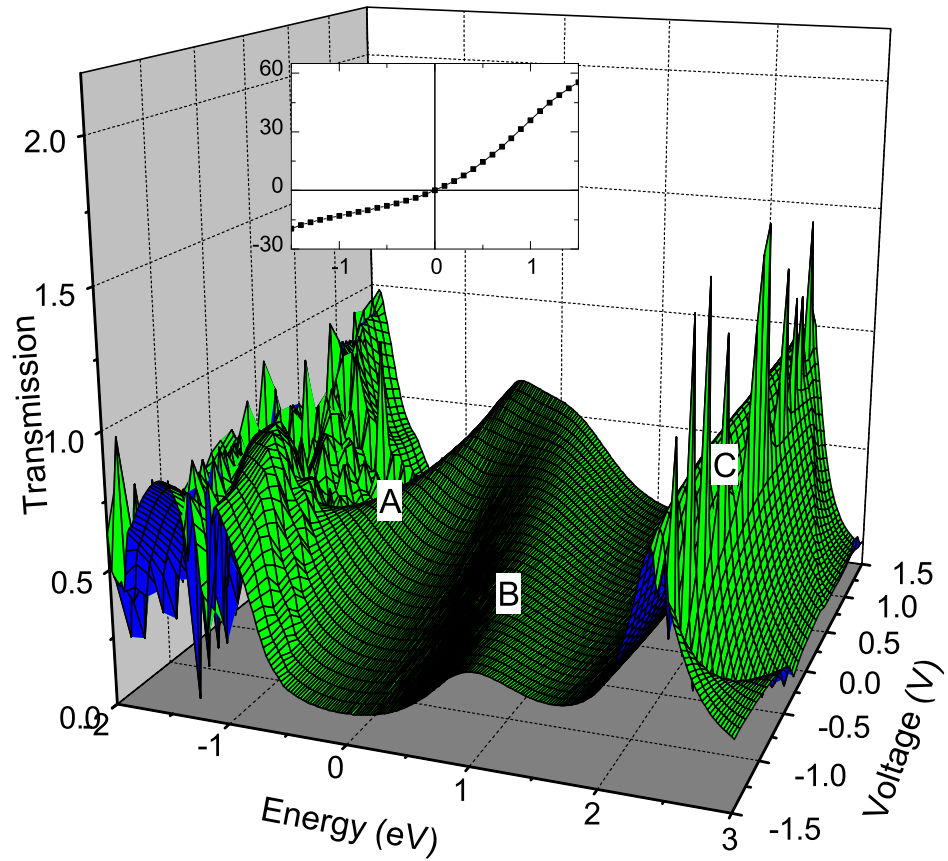


FIG. 5: Voltage-dependant transmission spectrum of the TBCT junction. Inset: current-voltage curve with voltage (in V) as the abscissa and current (in  $\mu\text{A}$ ) as the ordinate.

TABLE II: Energies (in eV) of the peaks A, B and C from Figure 5 for different values of the applied voltage (in V).

voltage	A	B	C
1.5	-0.4	0.0	2.4
0.5	-0.7	0.3	2.4
0.0	-0.9	0.5	2.4
-0.5	-1.3	0.7	2.4
-1.5	-1.5	1.0	2.4

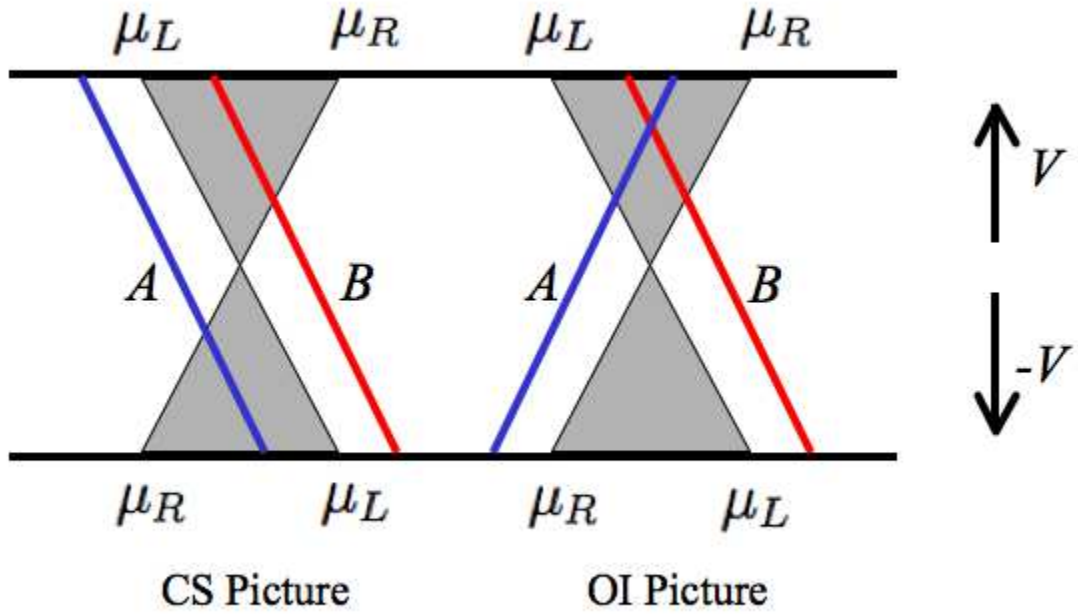


FIG. 6: Coupling strength (CS) and orbital interaction (OI) mechanisms for current rectification. The transmission from the shadow region contributes to current (see Equation (2)). Blue and red lines represent two transmission resonances  $A$  and  $B$ .